Journal of Power Sources 248 (2014) 1058–1066

Contents lists available at ScienceDirect

Journal of Power Sources

journal homepage: www.elsevier.com/locate/jpowsour

Studies on preventing Li dendrite formation in Li–S batteries by using pre-lithiated Si microwire anodes

M. Hagen [a,*], E. Quiroga-González [b], S. Dörfler [c], G. Fahrer [a], J. Tübke [a], M.J. Hoffmann [d], H. Althues [c], R. Speck [a], M. Krampfert [a], S. Kaskel [c], H. Föll [b]

[a] Fraunhofer Institute for Chemical Technology (ICT), Joseph-von-Fraunhofer-Str. 7, 76327 Pfinztal, Germany
[b] Christian-Albrechts-University of Kiel, Institute for Materials Science, Kaiserstraße 2, 24143 Kiel, Germany
[c] Fraunhofer Institute for Material and Beam Technology (IWS), Winterbergstraße 28, 01277 Dresden, Germany
[d] Karlsruhe Institute for Technology (KIT), Institute for Applied Materials–Ceramics in Mechanical Engineering, Haid-und-Neu-Straße 7, D-76131 Karlsruhe, Germany

HIGHLIGHTS

- Lithium dendrites greatly reduce the reliability of Li–S cells.
- Lithium dendrites can easily grow around or pierce conventional separators.
- Si microwire array anodes show high capacity and high coulometric efficiencies vs. Li.
- The performance of pre-lithiated Si anodes vs. S_8 cathodes depends on the electrolyte.
- Polysulfides/Li_2S and $LiNO_3$ should be added to the electrolyte of a Li_xSi_y–S_8 cell.

ARTICLE INFO

Article history:
Received 16 August 2013
Received in revised form
25 September 2013
Accepted 29 September 2013
Available online 14 October 2013

Keywords:
Lithium–sulfur
Dendrites
Si anode
sulfurcathode
Pre-lithiated electrodes
Battery

ABSTRACT

In this work, detailed studies on Li dendrite formation in Li–S Batteries are reported. Li dendrites can grow rapidly, may pierce through or can easily grow around the separator. Dendrites can even lead to short circuits when cathode and/or anode are wrapped with the separator. By replacing the Li metal anode with a pre-lithiated Si anode, these dendrite problems could be successfully prevented and were not observed for more than 200 cycles. The here used Si microwire array anodes are examined with ether and carbonate based electrolytes and different charging conditions vs. a Li metal counter electrode and demonstrate very high capacities matching the theoretical values.

Electrochemical pre-lithiated Si microwire array anodes are examined in full cells with binder free, sulfur infiltrated carbon nanotube cathodes (CNT-S) and various polysulfide or Li_2S containing electrolytes. The average polysulfide chain length and the presence of $LiNO_3$ in the electrolyte have a great impact on the cycle stability of the cell, next to the charging conditions.

1. Introduction

Li metal is theoretically the best possible choice for an anode material because of its low potential (−3.045 V vs. H_2/H^+) and its low density leading to a very high theoretical gravimetric capacity of 3862 mAh g^{-1}.

Li primary batteries like thionyl chloride, sulfuryl chloride or Li–MnO_2 have existed for several decades. Nevertheless, there are hardly any secondary batteries with Li metal anode due to safety reasons. The main drawback of Li metal anodes is the dendritic growth of Li during charge. The Li dendrites can pierce through the separator causing short circuits that may lead to severe thermal runaway or cell failure. Safety problems are additionally intensified through the low melting point of Li (180 °C). Furthermore dead/electrochemically inactive Li [1] and cycle efficiencies below 100% also lead to a necessary excess of Li metal in the cell to keep the obtainable capacity stable. Only the discovery of the intercalation principle for graphite led to modern rechargeable cells with Li-ions as charge carriers and to high stability for large cycle numbers [2].

To avoid safety problems in Li–S cells, Li-alloy anodes based on Sn [3,4] or Si [5–7] have been used. Si is of special interest, because

* Corresponding author. Tel.: +49 721 4640 716; fax: +49 721 4640 318.
E-mail address: markus.hagen@ict.fraunhofer.de (M. Hagen).

0378-7753/$ – see front matter © 2013 Elsevier B.V. All rights reserved.
http://dx.doi.org/10.1016/j.jpowsour.2013.09.144

it has a larger gravimetric capacity compared to Sn. Furthermore, it is a very abundant, cheap material and as the microelectronic industry is based on it, there are many standard techniques to process it in a very controlled manner. Self-standing Si microwire array anodes are one of the most viable Si anode approaches for practical applications, due to their high areal capacity, extraordinary mechanical stability and long cycle life [8]. Unfortunately, a Si based anode lowers the average discharge cell voltage significantly compared to Li metal (Li_2S–Si: 1.7–1.8 V; Li–S: ~2.15 V), thus decreasing the energy density on cell level greatly. Nevertheless, the obtainable cell energy density with a sulfur based cathode and a Si based anode of approximately 300 Wh kg^{-1} still exceeds the values of commercialized systems.

We would like to contribute to the high energy cell research by focussing on the safety aspect of Li metal anodes and by presenting test results of pre-lithiated Si microwire array anodes vs. binder free CNT-S cathodes with various electrolytes.

2. Experimental

2.1. Preparation of binder-free S-infiltrated CNT-electrodes

A 3D carbon nonwoven-based gas diffusion layer with a dimension of approximately 6 × 20 cm was dip coated with Al_2O_3 + a catalyst layer and used as substrate for the growth of CNTs by a CVD process. The detailed procedure is described elsewhere [9,10] with a process schematic in Ref. [10]. Li–S battery test results and properties of the CNT coated carbon structure electrodes including conductivity, surface area, performance with various sulfur, CNT loads and current densities are described in Ref. [11].

The electrodes were cut by a round punch hole with $d = 10$ mm. The sulfur infiltration was done in air by distributing sulfur powder homogenously on the electrode and by a subsequent melting step using a hot plate at 150 °C hot plate temperature. Fig. 1a (left) illustrates a SEM image of a CNT coated gas diffusion layer. CNT batches completely cover the carbon fibres of the substrate. Fig. 1a (right) shows the corresponding SEM:EDX image proving the homogenous sulfur distribution after the sulfur melt infiltration.

2.2. Preparation of Si microwire array anodes

The Si microwire array anodes were produced through various optimized etching and metal deposition steps, using a crystalline Si wafer as starting material. The distance from centre to centre of the Si microwires is 3 μm. This distance exactly compensates the theoretical volume expansion of Si (~300%) after complete lithiation, which is mainly radial [12]. The microwires have a diameter of 1 μm, a length of around 70 μm and are embraced by a copper current collector being directly galvanized around their top level. The Si microwire array electrode is binder free and consists of 100% active material (no conductive carbon). The detailed preparation process is described in Refs. [8,13,14]. Fig 1b shows a cross-section SEM image of a Si microwire array anode with galvanized Cu current collector.

For the full cell experiments the Si microwire array electrodes were charged and discharged vs. lithium metal for 10 cycles with 0.6 mA cm^{-2} between 0.1 and 0.7 V. The discharge time was limited to obtain 80% of the theoretical capacity as a maximum. In a subsequent final discharge step, the Si microwire array anodes were discharged without any limitations to obtain a pre-lithiated anode with the highest possible lithium fraction. The pre-lithiated Si microwire array anodes were then assembled vs. a binder-free CNT-S_8 cathode to obtain a full cell.

2.3. Cell assembly

Li metal (SA, 99.9% purity) was scraped with a ceramic knife to remove undesired surface layers and afterwards pressed through a calender to obtain a homogeneous and reproducible surface. Glass tube cells were used to allow the examination of the electrode stack and electrolyte. Commercial polypropylene separators with a thickness of approximately 25 μm and an average pore size between 30 and 40 nm were used. A defined amount of electrolyte, all with a water content below 20 ppm was pipetted on the separator. The following electrolytes were used:

- E1: 0.7 M LiTFSI in DME:DIOX (2:1, v:v) (SA, anhydrous) + 0.25 M $LiNO_3$ (ABCR 99.98%; metals basis).
- E2: Same composition as E1, but without $LiNO_3$
- E3: 10 ml E2 with polysulfides (0.1 g Li_2S + 0.25 g S_8)
- E4: 1 M $LiPF_6$ in EC:DMC (1:1, wt) (Merck)
- E5: 10 ml E1 with polysulfides (0.1 g Li_2S + 0.1 g S_8)
- E6: 10 ml E1 with 0.43 g Li_2S

The polysulfide containing electrolytes were created by adding the stated masses of S_8 (SA, >99.5%) and Li_2S (Rockwood Lithium, 99.9%) and mixing them with a Thinky ARE-250 Mixer. The assembly of the test cells was done in an argon-filled glove box (MBraun) with an O_2 and H_2O content below 1 ppm.

2.4. Test cell configurations

To examine Li dendrite creation or separator piercing, three different cell configurations were used. In the first configuration (Fig. 3a) two layers of separator ($d = 16$ mm) were wrapped around the Li metal anode ($d = 10$ mm), and in the second configuration (Fig. 3b) around the S cathode ($d = 10$ mm). Cells with shunts were closely examined with a light microscope.

To investigate whether the Li can also pierce the separator in the middle of the electrode area, a third cell configuration was developed (Fig. 4a). The electrode size and corresponding stainless steel

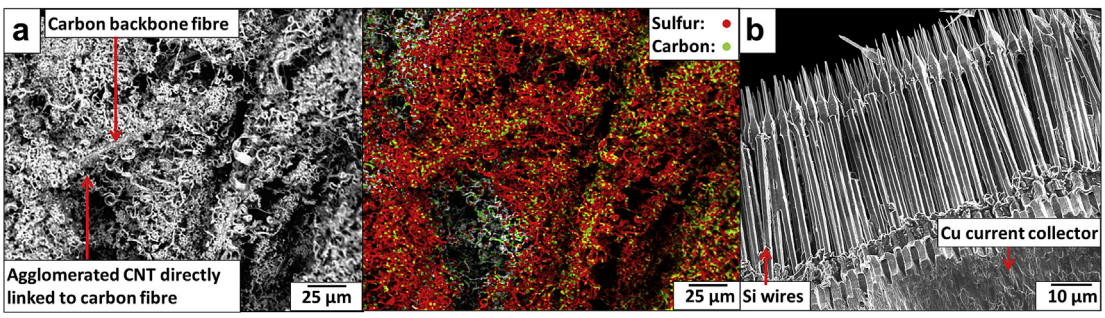

Fig. 1. a) Left: SEM image in top view of a sulfur infiltrated binder free CNT coated gas diffusion layer, right: corresponding SEM-EDX image and b) SEM image of a Si microwire array in side view.

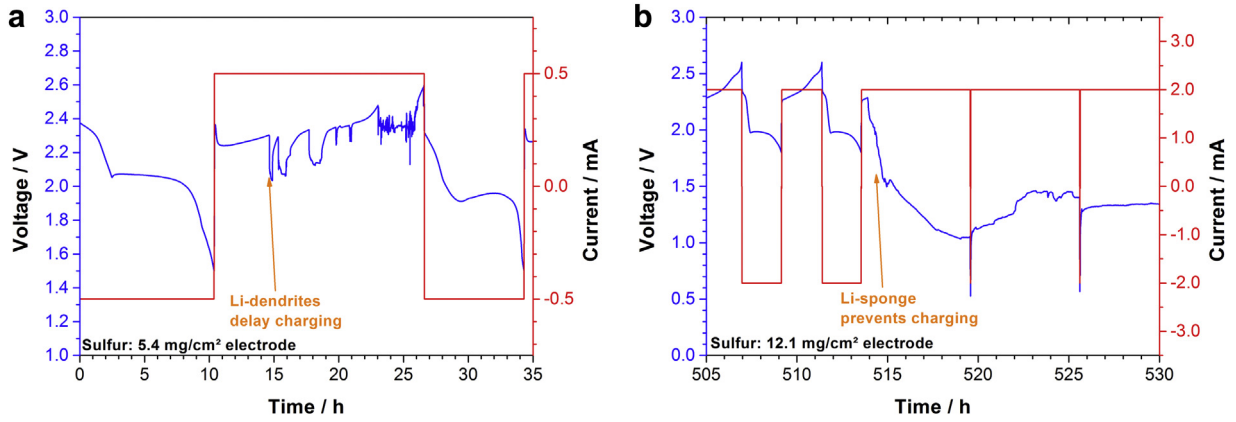

Fig. 2. Cycling voltage plots – effects of Li dendrites in Li–S cells (1.5–2.6 V). a) Small sized Li shorts delay charging b) Li sponge prevents charge and discharge.

contact disk were reduced to 0.5 cm^2 ($d = 8$ mm) and put inside an isolating polypropylene ring with $d = 11$ mm. Above the contact disks several layers of copper mesh with increasing mesh size were placed, to increase the surface on which Li can accumulate during charge. Li was pressed in the first layers of copper mesh. The separator ($d = 11$ mm) greatly overlapped the electrodes. Additionally the isolating polypropylene ring prevented the Li dendrite growth around the separator during charge.

2.5. Characterization

- The used cycle station was a Basytec CTS-LAB system. The Li–S cells were typically cycled between 1.5 and 2.6 V, the Li–Si half cells between 0.1 and 0.7 V or 0.1–1.0 V and the Li_xSi_y–S_8 full cells between 1.0 and 2.6 V or 1.2–2.6 V. The Si mass loads were always between 1.3 and 1.4 mg cm^2. The S_8 loads for the full cells tests were between 3.0 and 4.4 mg cm^{-2}. The starting current for the initial cycles was always 0.6 mA cm^{-2} (around C/9 referred to the Si mass) but may have been set to higher levels during the test depending on the experiment. All cells were cycled galvanostatically if not stated otherwise. For some experiments an additional potentiostatic step was added after the galvanostatic step in which the voltage was kept constant (Li–Si: 0.7 V; Li_xSi_y–S_8: 2.6 V) until the current was below C/20.
- Scanning electron microscope (SEM) micrographs were taken with a Zeiss type EVO MA 10 with a Peltier element cooled sample holder and wolfram cathode. EDX measurements were conducted with an Oxford Instruments X-Max.
- A Keyence VHX 100 light microscope was used to examine the lithium dendrites.

3. Results and discussion

3.1. Li sponge, dendrites and internal shorts/shunts

Li dendrites are a severe problem in Li–S cells since they frequently generate short circuits or shunts during charge. High electrode area capacities through high S loads, large separator

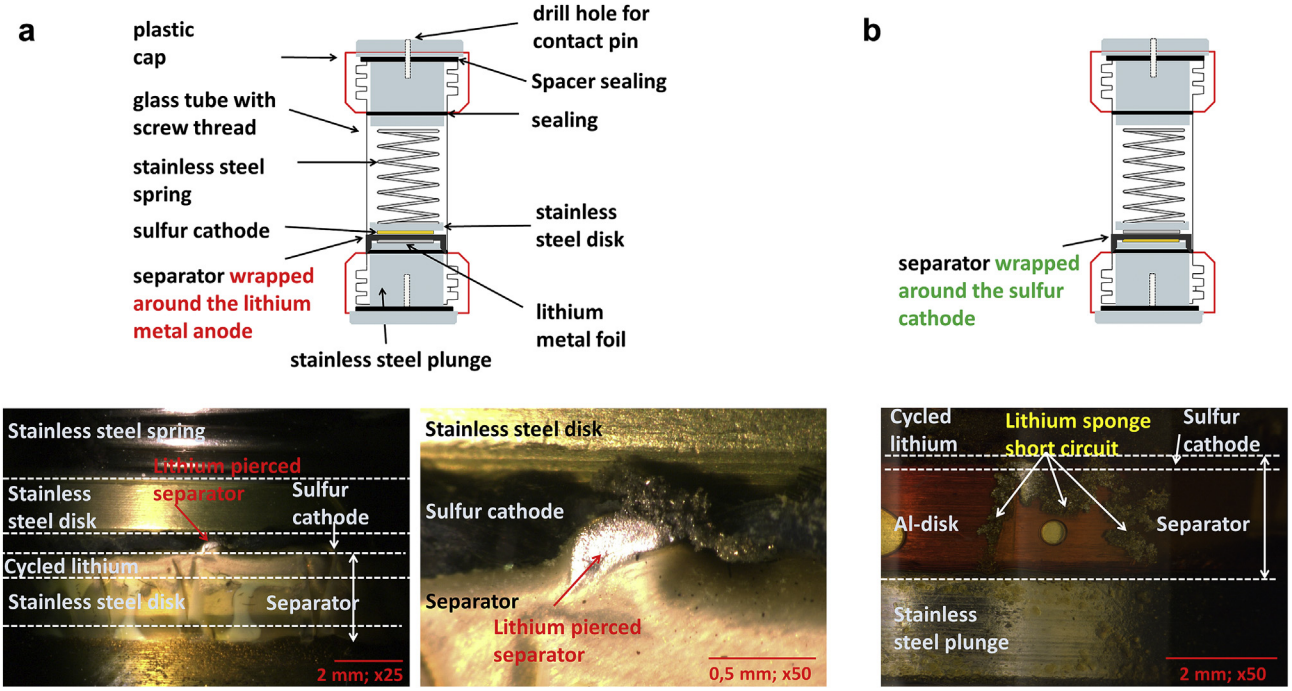

Fig. 3. Test cell configurations with corresponding post mortem light microscope pictures: a) Separator wrapped around the Li metal anode – Li pierced through separator and b) separator wrapped around the *S* cathode – Li sponge grown around separator.

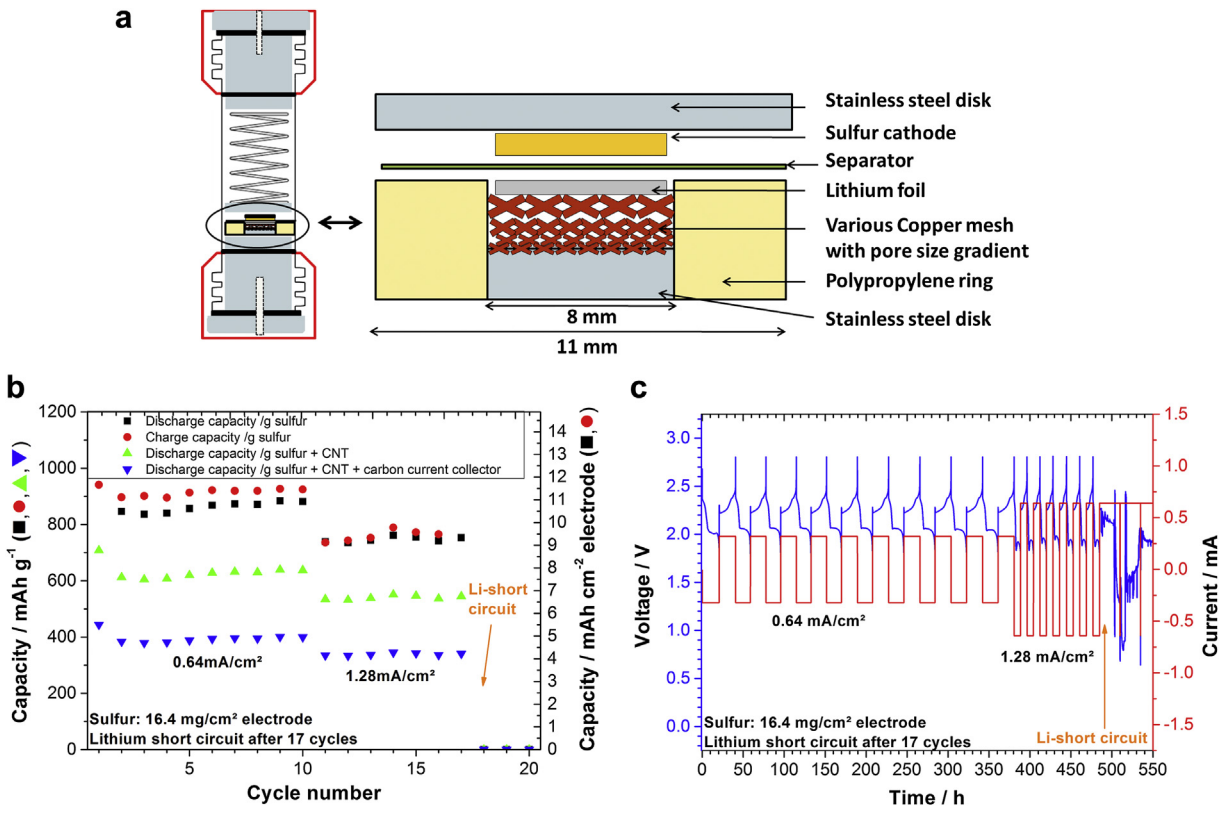

Fig. 4. a) Cell configuration: An isolating polypropylene ring prevents Li deposition in this area b) capacity over cycle number with corresponding cell configuration and c) corresponding cycling voltage plot.

pores, thin separators, a small separator/electrode overlap and a high porosity of the separator make it easier for Li dendrites to pierce through or grow around the separator. Fig. 2a shows a typical cycling voltage plot of a Li–S cell suffering dendritic or sponge-like Li growth that led to several voltage drops through local short circuits during charge. Having small sized Li shunts in the cell, a complete charge to the end of charge voltage may still be possible, but usually the Li shunts occur again in the next charging cycles, greatly reducing the efficiency. If the shunt has a bigger size (Fig. 2b), the cell voltage can drop below 1.0 V even during charge. In this case, a charge and discharge of the cell is impossible.

Since round transparent glass tube test cells were used for all Li–S tests, it was possible to discover Li shunts easily if they occurred at the edge of the electrode. Fig. 3a shows an image resulting from the experiment with the separator wrapped Li cell. Li pierced through the polypropylene separator and created a gap with a length of around 0.3 mm. Fig. 3b shows a cell with a separator wrapped S cathode. Here the Li sponge grew around the separator until it was in contact with the counter stainless steel contact. The Li sponge shunts developed a length of around 2 mm at several points around the electrode.

Fig. 4a shows the cell configuration to examine lithium penetration of the separator in the middle of the electrode with a corresponding plot of the capacity over cycle number (b) and the corresponding cycling voltage plot (c). A capacity drop after the first 10 cycles occurred due to the doubling of the current from 0.64 mA cm^{-2} to 1.28 mA cm^{-2}. After only 17 cycles, the capacity collapsed. The cycling voltage plot indicated the presence of Li shunts. Li may also pierce through a separator in the middle of an electrode after several cycles. Li induced shorts are therefore not constrained to the electrode edge.

To observe Li growth in-situ during the lithiation/delithiation process, a test cell with a separator wrapped CNT-S cathode (S load: 14.8 mg cm^{-2}) was assembled and charged between 1.8 and 2.8 V with 1.9 mA cm^{-2} current using E1 as electrolyte. A camera took pictures every two minutes over several days and cycles. The charge and discharge video of the corresponding cell can be seen in Video 1. The colour change of the electrolyte depends on the state of charge or the chain length of the dissolved polysulfides. A high concentration of short chain polysulfides (“discharged”) results in a yellow colour of the electrolyte. With increasing polysulfide chain length (“charged”) the colour of the electrolyte transforms to orange and later to red. The electrolyte colour change and polysulfide oxidation/reduction could clearly be observed around the positive electrode. In the video one can see that the electrolyte volume moves in the test cell during charge and discharge likely because of a volume change of the Li metal anode and the positive cathode.

Supplementary video related to this article can be found at http://dx.doi.org/10.1016/j.jpowsour.2013.09.144.

During charge, Li dendrites and sponge are continuously created at the Li metal anode, growing towards the separator wrapped CNT-S working electrode. During discharge, these Li structures shrink because of Li being transported to the CNT-S cathode. Nevertheless, after the complete discharge there is still some Li sponge left which is the preferred Li seed crystal for the next charge cycle. After several cycles, depending on the mass of the transported Li and therefore the active material mass, large Li sponge formations were created as can be seen in Fig. 3.

In summary, it could be demonstrated that Li has the ability to pierce through or to grow around one or two layers of typical commercial separators even with a small average pore size of 30–40 nm. Separator pockets used so far in small Li–S pouch

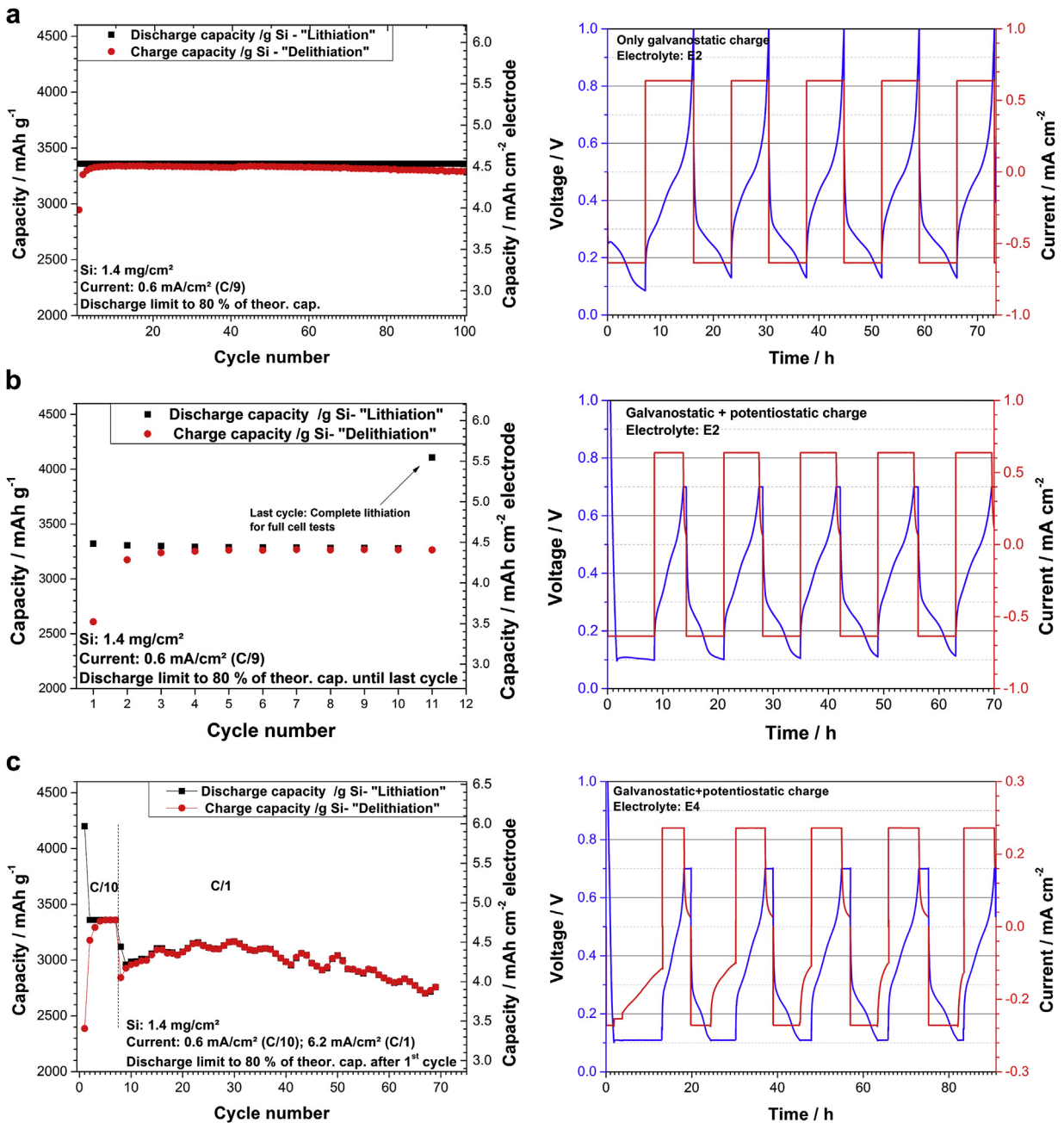

Fig. 5. Capacity over cycle number and corresponding cycling voltage plots of Si microwire array anodes vs. Li with different electrolytes and charge methods. The Si microwire array anodes consist out of 100% Si without any conductive carbon and polymer binder. E2: 0.7 M LiTFSI in DME:DIOX (2:1, v:v); E4: 1 M $LiPF_6$ in EC:DMC (1:1, wt).

cells can prevent the Li from growing around the separator but cannot prevent separator penetration. High sulfur loads greatly accelerate separator penetration. Nevertheless, decent S loads of at least 3 mg cm^{-2} are needed to overcome the energy density level of Li-ion intercalation electrodes. We suggest that complete new types of separators are essential for Li–S cells (or other secondary cells with a Li metal anode). The separator should have a small pore size (~30 nm or smaller), a high tortuosity (to resist penetration), a good wettability (to absorb the electrolyte) and a thickness of at least 25 μm. Ideally, the separator is Li^+ conductive and has no pores or has pores being too small to allow polysulfide migration or coatings, blocking the polysulfide shuttle.

3.2. Si microwire array anodes vs. Li

Si microwire array anodes were cycled vs. Li with electrolyte E2 (Fig. 5a, b) and E4 (Fig. 5c), without and with additional potentiostatic charge. The Si mass loads were approximately 1.4 mg cm^{-2} and the discharge time was set to limit the capacity to 80% of the theoretical value (3360 mAh g^{-1}_{Si}). This value was obtained with all three cells at a current of 0.6 mA cm^{-2}. The charge capacity (delithiation) of the first 3–5 cycles is lower with capacities between 2400–3300 mAh g^{-1}_{Si} before getting more and more aligned with the discharge capacity level. The loss of lithium in the first cycles corresponds to the creation of a SEI layer on the Si surface, which seems to be finished after cycle 3–5, being in good agreement with

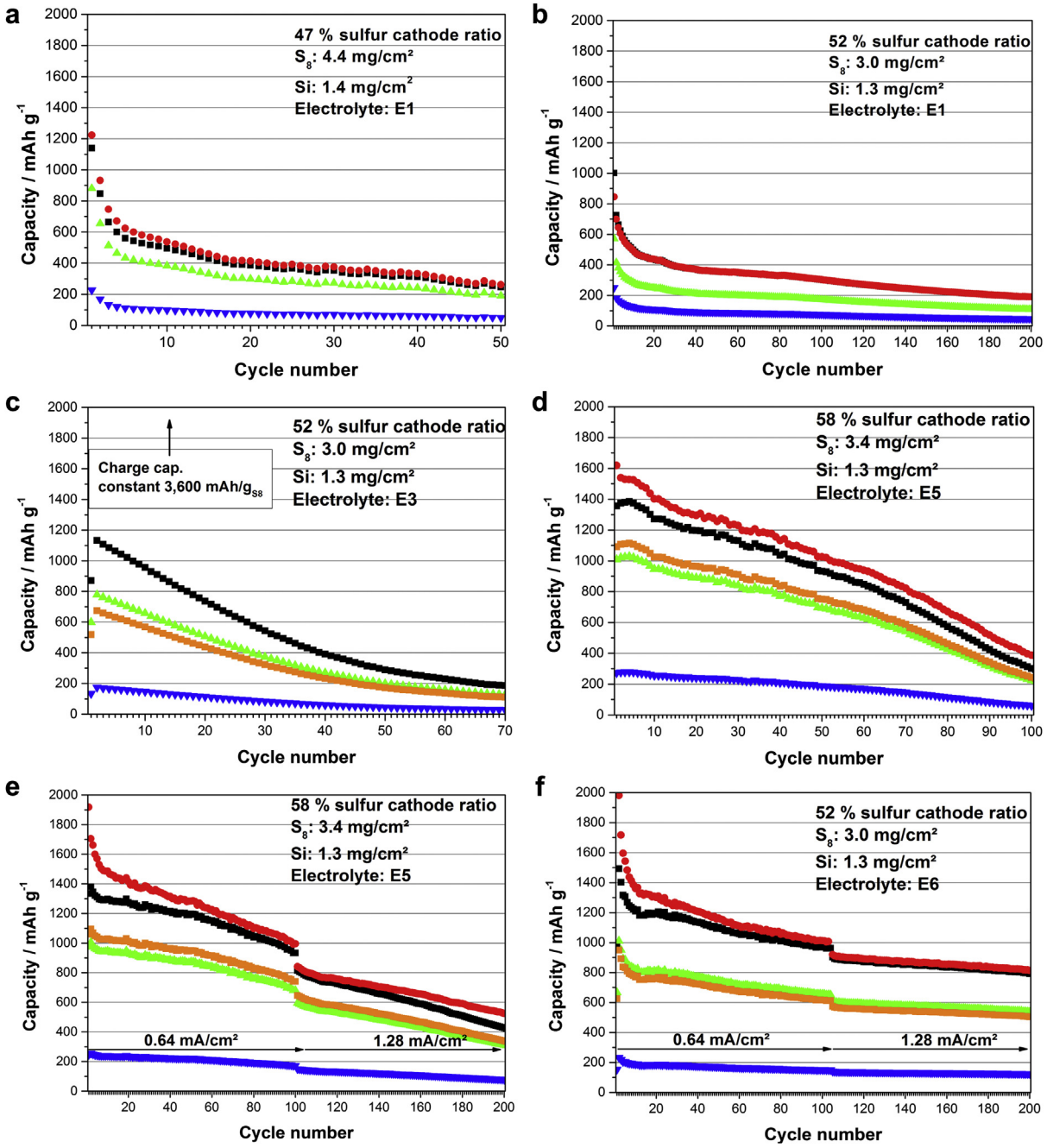

Fig. 6. Capacity over cycle number of a lithiated Si anode (Si = 1.35 mg cm^{-2}) vs. CNT-S cathode (S = 3.0–4.4 mg cm^{-2}) with various electrolytes. Current: 0.64 mA cm^{-2}. After 100 cycles, the current was set to 1.28 mA cm^{-2} for e) and f). d) Was also charged potentiostatically. ●: Charge capacity g^{-1} S_8, ■: Discharge capacity g^{-1} S_8, ■: Discharge capacity g^{-1} S_8 + PS, ▲: Discharge capacity g^{-1} S_8 + Si, ▼: Discharge capacity g^{-1} (S_8 cathode, including current collector + Si). All electrolytes base on 0.7 M LiTFSI in DME:DIOX (2:1, v:v): E1: +0.25 M $LiNO_3$; E3: no $LiNO_3$, +0.1 g Li_2S + 0.25 g S_8 (for 10 ml); E5: +0.25 M $LiNO_3$, +0.1 g Li_2S + 0.1 g S_8 (for 10 ml); E6: +0.25 M $LiNO_3$, +0.43 g Li_2S (for 10 ml).

Ref. [12]. When the cell with electrolyte E2 was charged only galvanostatically, there was a constant gap between charge and discharge capacity leading to coulometric efficiencies between 98.0 and 99.3% (Fig. 5a). An additional potentiostatic charge led to coulometric efficiencies of up to 99.5% (Fig. 5b). When the carbonate based E4 electrolyte was used, the coulometric efficiency was up to 99.8% even at the very high current of 6.2 mA cm^{-2} (Fig. 5c). Capacity oscillations observed at 6.2 mA cm^{-2} seem to be related to the change of the temperature, affecting the electrolyte's conductivity and viscosity during the day (every oscillation of capacity corresponds approximately to 1 day). Due to the high coulometric efficiency, carbonate based electrolytes would be favourable for a S_8–Li_xSi_y or Li_2S–Si full cell concept compared to ether based electrolytes. Unfortunately, the EC:DMC, or more generally, carbonate based electrolytes are not operational with S cathodes, because they show very low polysulfide solubility [15]. An exception are polyacrylonitrile–sulfur composite electrodes that are operable in carbonate based electrolyte and seem to have a different reaction mechanism which is not based on polysulfides and which is not yet completely understood [15,16]. Additionally, a polyacrylonitrile–sulfur cathode combined with a Si anode would not be an ideal high energy cell because of the low average

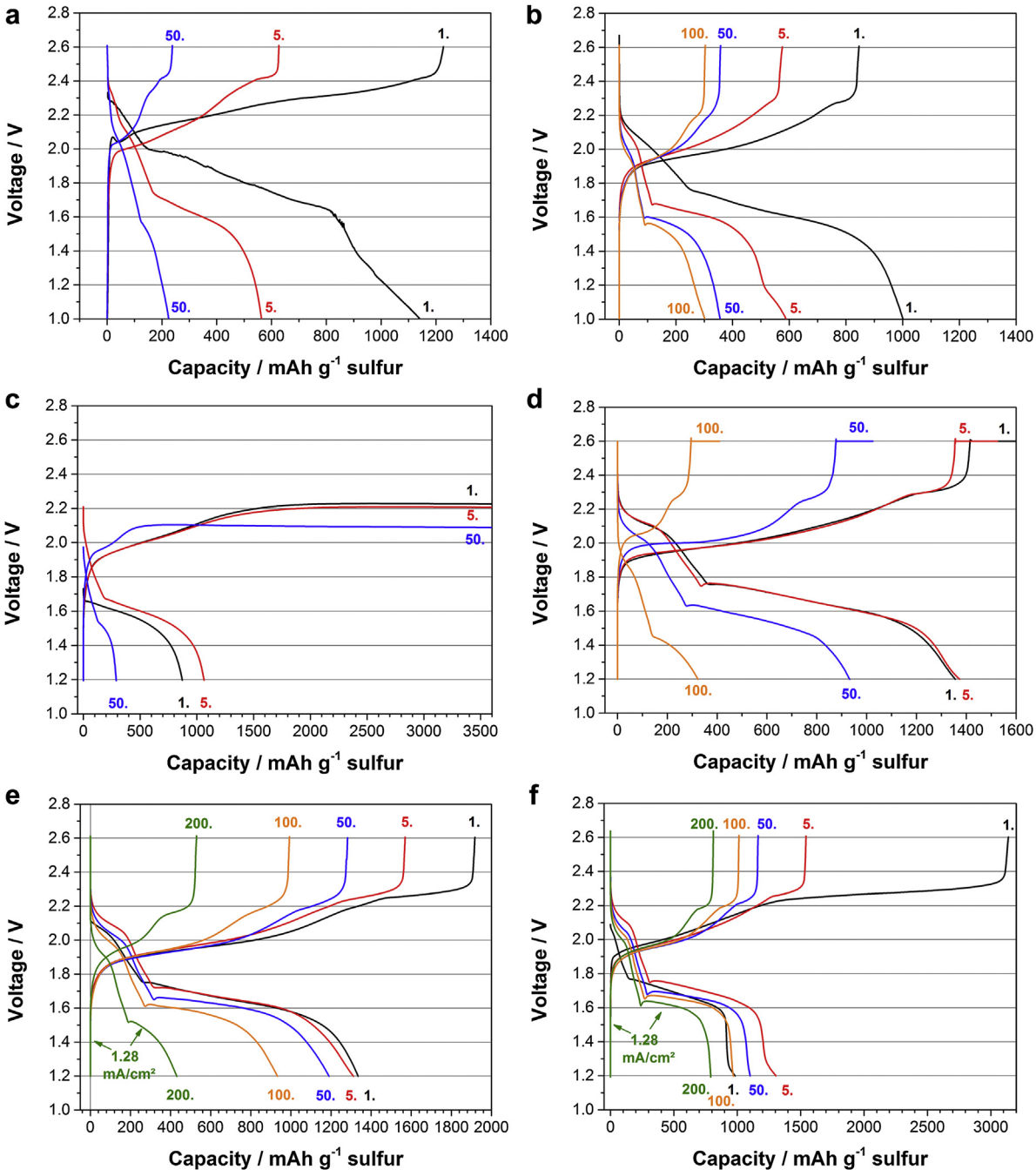

Fig. 7. Corresponding cycling voltage plots of Fig. 6 at 0.64 mA cm^{-2} at various cycles. Cycling voltage plot of cycle 200 in e) and f) at 1.28 mA cm^{-2}.

discharge cell voltage (~1.5 V) and a sulfur fraction regularly clearly below pure S cathodes [11]. Therefore, we suppose that Li_xSi_y–S or Si–Li_2S cells need to use ether based electrolytes at least at the cathode side.

The here examined Si microwire array anodes delivered perfectly stable capacities in all test cells vs. Li counter electrode because of their ideal design which compensated the stress of the Si volume change. Capacity fading is dependent on external parameters (e.g. high current densities) that affect the mechanical stress of the electrode. By limiting the lithiation capacity or by applying moderate currents (e.g. C/2) this stress is reduced and the cycle number can be kept relatively stable for hundreds of cycles.

3.3. Lithiated Si microwire array anodes vs. CNT-S cathode

Fig. 6 shows the capacity results of various binder free CNT-S cathodes with sulfur loads between 3.0 and 4.4 mg cm^{-2} vs. lithiated Si microwire array anodes with silicon loads of ~1.3 mg cm^{-2}. The Si microwire array anodes were charged/discharged for ten cycles vs. Li and electrochemically pre-lithiated before being assembled vs. the binder free CNT-S cathodes (compare Fig. 5b). The last cycle lithiation capacity was set to match 100% of the theoretical Si capacity to bring as much Li in the full cell as possible. The obtained capacity of 4200 mAh g^{-1}_{Si} matching the theoretical value shows again the high quality and perfectly tailored morphology of the Si microwire array anodes.

To provide extensive data for the full cell measurements the capacity was calculated for the S_8 mass (●: charge, ■: discharge), the S_8 mass + the polysulfide mass in the electrolyte (■: discharge), S_8 + Si mass (▲: discharge) and the complete S_8 cathode including the carbon current collector + Si mass (▼: discharge). The polysulfide's active mass added by the electrolyte was converted to the polysulfide's corresponding S_8 mass and added to the initial S_8 load on the electrode (■: discharge).

The corresponding charge and discharge profiles of the capacity diagrams (1st, 5th, 50th, 100th, 200th cycle) are demonstrated in Fig. 7. The capacity of the cells with electrolyte E1 (with $LiNO_3$, no polysulfides) faded quickly from around 900 mAh g_s^{-1} (g_s: S_8 active mass of the electrode) in the first cycle to around 300 mAh g_s^{-1} after around 50 cycles (Fig. 6a, b). One can suppose that this capacity drop could be induced by a lack of Li in the full cell combined with Li consumption e.g. because of SEI creation. But in contrary to the cell with a sulfur load of 4.4 mg cm^{-2} (Fig. 6a), the cell in Fig. 6b with 3.0 mg cm^{-2} had comparably more free Li and should therefore deliver a more stable capacity development. Nevertheless, the fast capacity drop in the first 20 cycles was almost comparable. To overcome this capacity drop, several electrolytes based on polysulfides were examined. The result shown in Fig. 6c was obtained by applying electrolyte E3 (no $LiNO_3$). It can be easily seen that the lack of $LiNO_3$ led to a shuttle mechanism. The higher voltage level of the Si anode compared to Li metal therefore does not prevent the shuttle mechanism which was already reported several years ago for Li–S cells [17]. The self-discharge of the shuttle was strong enough at the high voltage charge plateau (~2.2 V) to completely compensate the charge current of 0.64 mA cm^{-2}. Therefore, the charge cut off voltage of 2.6 V could not be reached (also compare Fig. 7c) and the charge was stopped automatically after a capacity of 3600 mAh g_s^{-1} was obtained. Additionally, the capacity still faded very quickly and was at around 300 mAh g_s^{-1} (or 200 mAh g_s^{-1} if the weight of the polysulfides is included) after 50 cycles. As a result, one can conclude that shuttle blocking additives or polysulfide blocking separators are necessary for Li_xSi_y–S_8 cells.

To examine whether the capacity drop can be reduced by charging methods, a test cell with electrolyte E5 (with $LiNO_3$ + polysulfides, Fig. 6d) was assembled. After reaching the cut off voltage (2.6 V) with a constant current of 0.64 mA cm^{-2}, a constant voltage charge was applied until the measured current was below 0.06 mA cm^{-2}. The initial capacity was approximately 1350 mAh g_s^{-1} (1100 mAh g_s^{-1} incl. polysulfides' weight). The capacity drop now was much slower but the capacity with around 300 mAh g_s^{-1} after 100 cycles was still low. Fig. 6e shows a reference cell, having the same active material load and electrolyte E5 - but no constant voltage charge was applied. The capacity was now comparably very stable with approximately 1200 mAh g_s^{-1} or 950 mAh g_s^{-1} if the polysulfides added to the electrolyte are taken into account. In contrast to the cells with Si anodes cycled vs. Li, showing better results with galvanostatic + potentiostatic charge (Fig. 5b), we believe that the constant voltage charge may have a negative effect on the electrolyte stability if a sulfur cathode is part of the system or more generally if polysulfides and/or $LiNO_3$ are part of the system. For the Li–S system several harmful electrolyte depletion products were already identified [18]. Comparing the voltage profiles of Fig. 7d and e, the voltage level of the discharge curves clearly sinks much stronger and the voltage level of the charge curves increases much stronger during cycling when the constant voltage charge is applied. This indicates a rising cell resistance which could be due to passivating layers [7] or maybe electrolyte decomposition.

After 100 cycles, the current was doubled to 1.28 mA cm^{-2}. The discharge capacity dropped to 800 mAh g_S^{-1} (620 mAh g_S^{-1} incl. polysulfides' weight) and was at 400 mAh g_S^{-1} after cycle 200. After cycle 120, a growing gap between charge and discharge capacity could be observed. This could be because of a stronger shuttle mechanism which especially increases the capacity contribution of the upper charge plateau (Fig. 7e, cycle 200). The stronger shuttle mechanism could be induced by temperature, which is unlikely because the labs were air-conditioned or by a complete consumption of the $LiNO_3$.

Fig. 6f shows the capacity development of a cell with electrolyte E6 ($LiNO_3$ + Li_2S). There is a great gap between the first cycle's charge and discharge capacity. This is caused by the Li_2S added to the electrolyte that has to be oxidized to long chain polysulfides or S_8 during charge and could not be further lithiated in the discharge before. After the first cycle, the capacity of the oxidized Li_2S products can be added to the regular active material. Consequently, the discharge capacity in the following cycles is much higher. The cycle stability of this cell showed the best performance and had a comparably very high capacity of 800 mAh g_S^{-1} (550 mAh g_S^{-1} incl. polysulfides' weight) after 200 cycles at a current of 1.28 mA cm^{-2}. Compared to the cell with electrolyte E5 the average discharge voltage level dropped much slowlier, indicating a lower increase of the cell impedance. Therefore, the creation of the passivating layer could be affected by the average polysulfides length in the electrolyte. Otherwise the Li consumed by this passivating layer could maybe also better be compensated by the addition of Li_2S, providing a higher Li content for the system.

Regarding the voltage profiles in Fig. 7, the average discharge voltage (upper plateau ~2.1 V, lower plateau ~1.65 V) is much lower compared to Li–S cells (upper plateau ~2.35 V, lower plateau ~2.1 V). Consequently, the possible cell energy density is significantly reduced. Therefore, we believe that the maximum energy density on cell level will be around 300 Wh kg^{-1} if the passive material's weight has the typical values. Additionally, a strong capacity fade along with a strong increase of the resistance is obvious as can be seen in Fig. 7a–d. Elazari et al. [7] reported on a growing anode surface layer consuming Li and increasing the resistance during cycling. Nevertheless, the effects of this passivating layer seem to be decreased by adding polysulfides/Li_2S and $LiNO_3$, indicated by the much more stable capacities and more constant voltage profiles shown in Figs. 6 and 7e, f.

4. Conclusion

Li metal anodes cause safety and reliability problems in Li–S cells. By several different electrode stack assembling ways and special test cells it could be demonstrated that Li can easily pierce or grow around commercial polypropylene separators. Therefore, completely new types of separators need to be developed for future Li secondary batteries. In contrast, Si anodes are much safer but either the S_8 cathode or the Si anode need to get lithiated to prepare a full cell. The herein used Si microwire array anodes demonstrated very high and stable capacities vs. Li with combined galvanostatic + potentiostatic charge and showed high coulometric efficiencies of up to 99.8% with carbonate based electrolytes after the SEI creation was finished. With ether based electrolytes the coulometric efficiency was up to 99.5%.

In order to obtain stable capacities with Li_xSi_y–S_8 cells it is recommended to add short chain PS into the electrolyte, ideally Li_2S. The known Li–S shuttle mechanism could also be reported for Li_xSi_y–S_8 cells and therefore could not be prevented by substituting Li with Si. Therefore a shuttle blocking additive like $LiNO_3$ is necessary to achieve a complete charge of the cell and to obtain stable capacities. Additionally, a combined galvanostatic + potentiostatic charge beneficially in Li–Si half cells should be avoided in Li_xSi_y–S_8 full cells, when polysulfides and $LiNO_3$ are part of the system. Li_xSi_y–S_8 cells with Li_2S and $LiNO_3$ additive in the electrolyte had the most stable capacity of up to 800 mAh g_S^{-1} after

200 cycles (550 mAh g_S^{-1} including PS weight) at a current of 1.28 mA cm^{-2}. It is likely that the higher Li fraction brought into the cell with a Li_2S additive compared to polysulfide additives is beneficial, if there is no excess of Li in the cell.

We believe that the used ether based electrolyte being unstable in Li–S cells is also not stable in Li_xSi_y–S_8 cells in the long term. In contrast to a Li metal anode which gets completely reduced and redeposited during cycling, the electrolyte decomposition should be more moderate with a Si anode. The unstable electrolyte in combination with passivating layers on the Si anode should be responsible for the capacity fade and therefore needs to be addressed with new types of electrolyte and/or additives.

Acknowledgements

This research was financed by the German Bundesministerium für Bildung und Forschung (BMBF) through the project STROM "AlkaSuSi – Alkali metal, sulfur and silicon". We are grateful for the support.

References

[1] J. O. Besenhard, Handbook of Battery Materials, Wiley VCH (1998), J. Yamaki, S. Tobishima, Rechargeable Li Anodes, 339–355.
[2] J.-M. Tarascon, M. Armand, Nature 414 (2011) 359–367.
[3] J. Hassoun, B. Scrosati, Angew. Chem. 122 (2010) 2421–2424.
[4] J. Hassoun, Y. Sun, B. Scrosati, J. Power Sources 196 (2011) 343–348.
[5] J. Hassoun, J. Kim, D. Lee, H. Jung, S. Lee, Y. Sun, B. Scrosati, J. Power Sources 202 (2012) 308–313.
[6] Y. Yang, M.T. McDowell, A. Jackson, J.J. Cha, S.-S. Hong, Y. Cui, Nano Lett. 10 (4) (2010) 1486–1491.
[7] R. Elazari, G. Salitra, G. Gershinsky, A. Garsuch, A. Panchenko, D. Aurbach, Electrochem. Commun. 14 (2012) 21–24.
[8] E. Quiroga-González, J. Carstensen, H. Föll, Electrochim. Acta 101 (2013) 93–98.
[9] S. Dörfler, A. Meier, S. Thieme, P. Németh, H. Althues, S. Kaskel, Chem. Phys. Lett. 511 (2011) 288–293.
[10] S. Dörfler, M. Hagen, H. Althues, J. Tübke, S. Kaskel, M.J. Hoffmann, Chem. Commun. 48 (2012) 4097–4099.
[11] M. Hagen, S. Dörfler, P. Fanz, T. Berger, R. Speck, J. Tübke, H. Althues, M.J. Hoffmann, C. Scherr, S. Kaskel, J. Power Sources 224 (2013) 260–268.
[12] E. Quiroga-González, J. Carstensen, H. Föll, Materials 6 (2013) 626–636.
[13] E. Quiroga-González, E. Ossei-Wusu, J. Carstensen, H. Föll, J. Electrochem. Soc. 158 (2011) E119–E123.
[14] H. Föll, J. Carstensen, E. Ossei-Wusu, A. Cojocaru, E. Quiroga-González, G. Neumann, J. Electrochem. Soc. 158 (2011) A580–A584.
[15] L. Wang, X. He, J. Li, M. Chen, J. Gao, C. Jiang, Electrochim. Acta 72 (2012) 114–119.
[16] W. Wei, J. Wang, L. Zhou, J. Yang, B. Schumann, Y. NuLi, Electrochem. Commun. 13 (2011) 399–402.
[17] Y.V. Mikhaylik, J.R. Akridge, J. Electrochem. Soc. 151 (11) (2004) A1969–A1976.
[18] Y. Mikhaylik, I. Kovalev, R. Schock, K. Kumaresan, J. Xu, J. Affinito, ECS Trans. 25 (35) (2010) 23–34.